STEM CELLS TRANSLATIONAL MEDICINE®

ENABLING TECHNOLOGIES FOR CELL-BASED CLINICAL TRANSLATION

Epicardium-Derived Cells Formed After Myocardial Injury Display Phagocytic Activity Permitting In Vivo Labeling and Tracking

ZHAOPING DING,[a] SEBASTIAN TEMME,[a] CHRISTINE QUAST,[a] DANIELA FRIEBE,[a] CHRISTOPH JACOBY,[a] KLAUS ZANGER,[b] HANS-JÜRGEN BIDMON,[c] CHRISTOPH GRAPENTIN,[d] ROLF SCHUBERT,[d] ULRICH FLÖGEL,[a] JÜRGEN SCHRADER[a]

Key Words. Myocardial infarction • ^{19}F-Magnetic resonance imaging • Perfluorocarbon nanoemulsions • Epicardium-derived progenitor cells • Phagocytosis

[a]Department of Molecular Cardiology, [b]Center of Anatomy and Brain Research, Department of Anatomy I, and [c]Cécile and Oskar Vogt-Institute for Brain-Research, Heinrich Heine University, Duesseldorf, Germany; [d]Department of Pharmaceutical Technology and Biopharmacy, Albert Ludwig University, Freiburg, Germany

Correspondence: Jürgen Schrader, M.D., Department of Molecular Cardiology, University of Duesseldorf, Moorenstrasse 5, 40225 Duesseldorf, Germany. Telephone: 49 211 81 10527; E-Mail: schrader@uni-duesseldorf.de

Received July 20, 2015; accepted for publication January 13, 2016; published Online First on April 7, 2016.

1066-5099/2016/$20.00/0

http://dx.doi.org/10.5966/sctm.2015-0159

ABSTRACT

Epicardium-derived cells (EPDCs) cover the heart surface and can function as a source of both progenitor cells and trophic factors for cardiac repair. Currently, EPDCs cannot be conveniently labeled in vivo to permit imaging and cell tracking. EPDCs formed after myocardial infarction (MI) preferentially take up a perfluorocarbon-containing nanoemulsion (PFC-NE; 130 ± 32 nm) injected 3 days after injury, as measured by ^{19}F-magnetic resonance imaging (^{19}F-MRI). Flow cytometry, immune electron microscopy, and green fluorescent protein (GFP)-transgenic rats (only immune cells, but not epicardial cells, are GFP$^+$) demonstrated that PFC-containing EPDCs are nonhematopoietic (CD45$^-$/CD11b$^-$) but stain positive for markers of mesenchymal stem cells such as platelet-derived growth factor receptor α (PDGFR-α) CD73, CD105, and CD90. When rhodamine-coupled PFC-NE was used, we found that ρ^+ vessel-like structures formed within the infarcted myocardium, comprising approximately 10% of all large vessels positive for smooth muscle actin (SM-actin). The epicardial cell layer, positive for Wilms' tumor 1 (WT-1), PDGFR-α, or KI-67, was shown to be well capillarized (293 ± 78 capillaries per mm^2), including fenestrated endothelium. Freshly isolated EPDCs were positive for WT-1, GATA-4, KI-67, and FLK-1 (75%), PDGFR-α (50%), and SM-actin (28%) and also exhibited a high capacity for nanoparticle and cell debris uptake. This study demonstrates that EPDCs formed after MI display strong endocytic activity to take up i.v.-injected labeled nanoemulsions. This feature permitted in vivo labeling and tracking of EPDCs, demonstrating their role in myo- and vasculogenesis. The newly discovered endocytic activity permits in vivo imaging of EPDCs with ^{19}F-MRI and may be used for the liposomal delivery of substances to further study their reparative potential. STEM CELLS TRANSLATIONAL MEDICINE *2016;5:639–650*

SIGNIFICANCE

The present study reports that epicardium-derived cells (EPDCs) formed after myocardial infarction can specifically endocytose nanoparticles in vivo and in vitro. This novel feature permitted in vivo targeting of EPDCs with either a perfluorocarbon-containing or rhodamine-conjugated nanoemulsion to track migration and fate decision of EPDC with ^{19}F-magnetic resonance imaging and fluorescence microscopy. The liposomal nanoemulsions used in the present study may be useful in the future as a nanomedical device for the delivery of substances to direct cell fate of EPDCs.

INTRODUCTION

The epicardium encapsulating the heart functions as a source of multipotent progenitor cells and paracrine factors essential for cardiac development, but becomes postnatally quiescent [1]. Lineage tracing experiments by drug-induced Cre/Lox fate-mapping technique in adulthood indicated that myocardial infarction (MI) activates epicardial cells to respond by an epithelial mesenchymal transition, forming epicardium-derived cells (EPDCs), which contribute to coronary vascular precursors, fibroblasts, and cardiomyocytes in an analogous manner to their embryonic counterparts [2]. In response to injury, EPDCs reactivate the expression of cardiac embryonic genes such as Wilms' tumor 1 (WT-1) and T-box 18, expand in number, and migrate into underlying myocardium [3], where they can form smooth muscle cells [4], endothelial cells, and fibroblasts [3] or, to a small extent, differentiate into cardiomyocytes when primed with thymosin β4 [2]. More recently, EPDCs have been shown to be a relatively heterogeneous cell population with angiogenic support and a noncellular contribution of the extracellular matrix [5]. Apart from their

cellular contribution, the epicardium can also modulate myocardial injury by secreting paracrine factors [6], one being epicardial hypoxia inducible factor, which promotes the invasion of vascular precursor cells into the heart [7]. Together, these findings indicate that EPDCs are key players in cardiac repair, and further understanding of their biology might offer new therapeutic strategies for the treatment of ischemic heart disease and heart failure.

Analysis of lineage specification of EPDCs would require a cell-specific labeling for tracking, to follow-up cell fate decision and their functional contribution to tissue repair. Noninvasive imaging of progenitor cells has been used in the past, not only to confirm cell delivery, but also to study the mechanisms of cell fate specification, migration, and survival after in vivo transplantation [8]. Thus, imaging techniques could be a valuable tool to track stem cells by real-time information, and so far various modalities, including magnetic resonance imaging (MRI), x-ray/computed tomography, and positron emission tomography (PET) have been used. The ideal imaging system should not use ionizing radiation, but provide high contrast as well as high special and temporal resolution. Among the magnetic resonance (MR)-based techniques, supraparamagnetic iron oxide (SPIO), and ultrasmall supraparamagnetic iron oxide have been widely used. Bulte and Kraitchman showed migration of stem cells in a reperfused dog infarction model over 8 weeks in the peri-infarct region [9]. Although the presence of hypointensities on MRI initially may reflect the number of injected cells, concern has been raised that at a later stage, it may reflect uptake of nanoparticles released from the dead cells by phagocytic cells. In addition, hypointensities created by SPIO-labeled cells may compromise visualization of the underlying anatomy. To overcome this problem, Ahrens et al. in 2003 reported using perfluorocarbons (PFCs) for in vivo cell tracking together with ^{19}F-MRI, when cells before injection were labeled ex vivo [10]. Because there is little native fluorine in the body together with the exquisite sensitivity of the fluorine nucleus, this creates hotspot MR images similar to PET imaging. This advantageous feature of perfluorocarbons in combination with ^{19}F-MRI was used by our group to image monocytes/macrophages infiltrating into the infarcted heart [11]. To this end, perfluorocarbons were injected intravenously to preferentially label circulating monocytes. Since these initial studies, noninvasive inflammation imaging with ^{19}F-MRI has emerged as a powerful technique for the in vivo tracking of monocytes and was successfully applied in various animal disease models, such as myocarditis [12, 13], arthritis [14], transplant rejection [15], and ventricular remodeling [16].

In the present study, we report the novel observation that PFC nanoemulsions (PFC-NEs) are avidly taken up by EPDCs in vivo and in vitro. Liposomal nanoemulsions thus constitute a delivery system to EPDCs formed by the infarcted heart and thereby allow their migration into the injured tissue to be followed by either fluorescence microscopy or ^{19}F-MRI.

Materials and Methods

Expanded Materials and Methods are found in the supplemental online data.

Animal Experiments

Animal experiments were approved by the Landesamt für Natur, Umwelt und Verbraucherschutz Nordrhein-Westfalen (LANUV) of Nordrhein-Westfalen. MI in either male Wistar rats or green fluorescent protein (GFP)-transgenic rats (250–300 g) [17] was induced by the ligation of left coronary descending artery in mechanically ventilated rats with isoflurane (1.5% [vol/vol]; Abbott, Chicago, IL, http://www.abbott.com). The occlusion was kept for 60 minutes (ischemia) and released (reperfusion) before the chest was closed. At the indicated time points (2nd or 4th days), a bolus injection of 2 ml of perfluoro-15-crown-5 ether nanoemulsions (10%) was given intravenously. To analyze the PFC-NE kinetics, blood samples were taken immediately (1 minute) and at various time points up to 24 hours (supplemental online Fig. 2), and plasma PFC-NEs were measured. To study the dynamics of epicardial labeling, 2 ml of rhodamine-coupled PFC-NEs (ρ-PFC-NE) was injected 3 days after ischemic injury. Heart samples were removed at 12 hours and 4 and 11 days after injection. In another series of experiments, clodronate liposomes (Encapsula NanoSciences, Brentwood, TN, http://www.encapsula.com) were injected i.v. (25 mg/kg) on day 4, and epicardial thickness was analyzed on day 7. Heart samples were preserved in Tissue-Tek (Klinipath, Duiven, The Netherlands, http://www.klinipath.nl) for further immunohistological analysis.

MRI

Data were recorded on a Bruker Avance III 9.4 Tesla Wide Bore (89 mm; Bruker, Billerica, MA, https://www.bruker.com) nuclear MR spectrometer operating at frequencies of 400.2 MHz for ^{1}H and 376.5 MHz for ^{19}F measurements and Paravision (version 5.1) as operating software essentially as described [11, 18]. Rat in vivo experiments were carried out by using a Bruker microimaging unit (Mini 0.5) equipped with actively shielded gradient sets (capable of 0.3 Tesla per meter maximum gradient strength and 150-μs rise time at 100% gradient switching) and a 30 $\times$ 40 mm^2 surface coil tunable to ^{1}H and ^{19}F with a penetration depth of approximately 20 mm. Rats were anesthetized with 1.5% isoflurane and were kept at 37°C. For functional and morphological analysis, cine movies of rat hearts were acquired in short axis orientation using an ECG- and respiration-gated fast imaging cine sequence with steady-state free precession. Cine loops were taken in 128 segments from a field of view (FOV) of 25.6 $\times$ 38.4 mm^2 and an in-plane resolution of 0.1 $\times$ 0.15 mm^2 after zero-filling (at 1 mm slice thickness) with a flip angle of 25°, echo time (TE) of 1.5 milliseconds, and a repetition time (TR) of approximately 12 milliseconds (acquisition time per slice for one cine sequence, 1.5 minutes). After recording of anatomical reference scans the coil was tuned to ^{19}F and corresponding ^{19}F MR images were taken with a multislice rapid acquisition with relaxation enhancement (RARE) sequence (TE, 5.5 milliseconds; TR, 2500 milliseconds; RARE factor 32; matrix 64 $\times$ 64; averages 256; acquisition time 21 minutes). For superimposing images from the two nuclei, the "hot iron" color table was applied to ^{19}F images. To fade out the background noise from ^{19}F images a constant threshold was applied to ^{19}F data.

Ex vivo MRI was carried out essentially as described previously [14]. A Bruker microimaging unit (Micro 2.5) equipped with an actively shielded 40-mm gradient set (capable of 1 T/m maximum gradient strength and 110 μs rise time at 100% gradient switching) was used. Explanted rat hearts were fixed in phosphate buffered paraformaldehyde (4%) and embedded in agarose within a 10-ml glass snap-cap vial, which was carefully fixed in the center of a 25-mm birdcage resonator tunable to ^{1}H or ^{19}F. After acquisition of morphological ^{1}H images, the resonator was tuned to ^{19}F, and anatomically matching ^{19}F images were recorded by using a three-dimensional (3D) RARE sequence (RARE factor 32, 25.6 $\times$ 25.6 $\times$ 20 mm^3, matrix 64 $\times$ 64 $\times$ 20, resulting in an in-plane voxel size of 0.2 $\times$ 0.2 mm^2 after zerofilling; slice thickness, 1 mm; TR, 2.5 s; TE, 4.78 milliseconds; 8 averages; acquisition time, 13.20 minutes). For merging of ^{1}H and

^{19}F data, again the hot iron color look-up table of Paravison was applied to ^{19}F MR images.

Isotropic high-resolution 3D datasets were acquired from a FOV of 20 × 20 × 20 mm^3 by using matrices of 256 × 256 × 256 for both ^{1}H and ^{19}F. For further processing, reconstructed ^{1}H and ^{19}F image stacks were imported into the 3D visualization software Amira (Mercury Computer Systems, Reston, VA, https://www.mrcy.com). ^{1}H signals were associated to the respective anatomical structures by using the Segmentation Editor of Amira. For segmented areas, individual surfaces were calculated with unconstrained smoothing. Subsequently, surface views with a semitransparent display using a "fancy α" were created. For overlay, anatomic corresponding ^{19}F data were volume rendered by the Voltex Module of Amira. The default color map (red) and rgba lookup mode were used for visualization, and the resulting projection from the "shining" data volume was computed by using an intensity range of 5,000–30,000. Fade-in of the projection and concomitant rotation of the surface views were coordinated with the DemoMaker of Amira.

Isolation of EPDCs

EPDCs were isolated by enzymatic digestion of heart surface. In brief, after being rinsed of blood, the hearts were immerged in a collagenase-containing solution (1,200 IU/ml; Biochrom, Cambridge, U.K., http://www.biochrom.co.uk) and gently rotated (60 rpm) at 37°C for 20 minutes. The resulting cell suspension was passed through a 40-μm cell strainer (BD Falcon), centrifuged, and resuspended for further analysis.

Cytospin and Immunostaining

Freshly isolated epicardial cells were magnetically depleted of myeloid cells (CD45-positive) by using microbeads (Miltenyi Biotec, San Diego, CA, http://www.miltenyibiotec.com). The resulting CD45-free cell suspension was centrifuged to make cells adhere to a poly-L-lysine-coated slide. After fixation, cells were permeabilized and incubated with primary antibodies against WT-1, GATA-4, platelet-derived growth factor receptor α (PDGFR-α), FLK-1 (all 1:100; Santa Cruz Biotechnology, Santa Cruz, CA, http://www.scbt.com), smooth muscle actin (SM-actin; 1:100; EMD Millipore, Billerica, MA, http://www.millipore.com), or KI-67 (1:100; Dako, Carpinteria, CA, http://www.dako.com) at 4°C overnight. After washing, fluorescein isothiocyanate (FITC)-coupled secondary antibodies were added, and nuclei were counterstained by 4′,6-diamidino-2-phenylindole (DAPI; Sigma-Aldrich, St. Louis, MO, http://www.sigmaaldrich.com). Micrographs were acquired with a fluorescent microscope (BX 61; Olympus, Tokyo, Japan, http://www.olympus.co.jp), and percentages of positive cells in relation to total cells were counted.

Flow Cytometry

The freshly isolated cells were fixed and stained with primary antibodies against PDGFR-α (1:100; Santa Cruz Biotechnology) and CD73 (1:100; BD, Franklin Lakes, NJ, http://www.bd.com) and appropriate secondary antibodies (Invitrogen, Carlsbad, CA, http://www.invitrogen.com). For CD105 and CD90 staining, cells were stained with CD45-allophycocyanin (CD45-APC), Cy7/CD11b-APC, and CD90-FITC (1:100; eBioscience, San Diego, CA, http://www.ebioscience.com) or CD105-Alexa 647 (1:100; Bioss Antibodies, Woburn, MA, http://biossusa.com). To determine the amount of rhodamine-labeled cells, staining with CD45-APC-Cy7 and CD11b-APC was conducted. Cells were analyzed with a fluorescence-activated cell sorting Canto II (BD Biosciences, San Jose, CA, http://www.bdbiosciences.com) or LSR Fortessa (BD Biosciences) for rhodamine detection.

Endocytic Properties of EPDCs In Vitro

The CD45-negative cell population was exposed to either 1% FITC-coupled PFC-NE or PKH26-labeled apoptotic cells induced by treatment of 2 μM staurosporine (Sigma-Aldrich) at 37°C or 4°C for various time periods from 5 to 120 minutes. Mean fluorescence intensity (MFI) of cellular PFC-NE uptake was measured by flow cytometry (Canto II; BD Bioscience). For comparison, the endocytic capacity of CD45-positive and CD11b/c-positive blood monocytes was assessed in parallel.

Heart Tissue Histology and Immunostaining

Cryosections (8 μm) were air-dried, and fluorescence images were immediately recorded without further processing because of water solubility of ρ-PFC-NEs. For quantification of MFI, eight randomly selected fields from both epicardial layer and injured myocardium in each midventricular region were analyzed. MFI in the region of interest (ROI) was estimated in three randomly selected areas. The total number of rhodamine-positive vessel-like structures was estimated and related to total SM-actin-positive vessels stained in the adjacent sections.

For immunostaining, tissue slices were fixed for 10 minutes in Zamboni fixative. The primary antibodies—including anti-SM-actin (1:400; Chemicon), anticardiac troponin T (cTnT, 1:400; Thermo Scientific, Oakwood Village, OH, http://www.thermoscientific.com), rabbit anti-KI-67 (1:400; Thermo Scientific), and anti-WT-1 (1:100; Santa Cruz Biotechnology), as well anti-PDGFR-α (1:100; Santa Cruz Biotechnology)—were incubated overnight at 4°C. After three wash steps, the FITC-labeled secondary antibodies (1:100, Dako) were used, and nuclei were counterstained with DAPI. Percentages of positive cells in relation to total cells (DAPI-positive) were derived from five individual sections at ×20 magnification.

In the experiments for colocalization, the modified fixation and permeabilization procedure was used. For detection of cell surface antigen, cryosections (15–20 μm) were incubated without permeabilization steps. For intracellular staining, samples were mildly permeabilized with 0.1% saponin for 10 minutes, and immunostaining was performed as described above. Pictures were acquired by using a confocal florescent microscope (Olympus, Fluoview 1000).

Transmission Electron Microscopy and Immune Electron Microscopy

For transmission electron microscopy (TEM) analysis, tissue samples were first fixed in 4% paraformaldehyde at 4°C overnight and then treated with 2% osmium tetroxide for 60 minutes. After fixation, tissue blocks were dehydrated in a graded series of acetone and embedded in Spurr's medium for ultrathin sections (80 nm; Ultracut; Reichert, Depew, NY, http://www.reichert.com). After being stained with uranyl acetate and lead citrate, the slices were examined by electron microscopy (H 600; Hitachi, Tokyo, Japan, http://www.hitachi.com), and digital images were acquired with a Gatan camera system and analyzed with Digital Micrograph Analyzing software (Gatan, Pleasanton, CA, http://www.gatan.com).

For immune electron microscopic examination, heart samples were fixed with Zamboni fixative overnight at 4°C and then sliced into ~900-μm sections by using a brain mold (ASI Instruments, Warren, MI, https://asi-instruments.com). After blocking

and fixation steps, primary antibodies—either anti-CD 11b/c (1:200) or anti-WT-1 (1:200)—were incubated, followed by biotinylated secondary antibody incubation (1:500; Dianova, Hamburg, Germany, http://www.dianova.com) for 48 h at 4°C. The tissue stripes were then polymerized for 3 days at 60°C and mounted on blocks and polymerized again. Ultrathin sections were cut, and electron microscopic evaluation was performed without further contrast enhancement by using an EM 902-A (Zeiss, Stuttgart, Germany, http://www.zeiss.com).

Size Distribution of PFC-NEs

The size distribution of PFC-NEs in vitro was determined by Zetatrac (Particle Metrix, Meerbusch, Germany, https://www.particle-metrix.de) as described previously [11]. In vivo size distribution was derived into eight individual TEM pictures of vesicular structures present within epicardial cells.

Statistical Analysis

Data are presented as means $\pm$ SD. One-way analysis of variance was used to compare the thickness of the epicardial layer and MFI in the heart sections at the different time points (after 12 hours [D4], 4 days [D7], and 10 days [D14]). Differences were considered significant at $p < .05$. The Prism software package (Version 5.0) was used for the statistical analysis.

RESULTS

Labeling Epicardial Cells After MI With PFC Nanoemulsions

We have previously reported a technique for visualizing local inflammatory processes by ^{19}F MRI using in vivo tagging of circulating monocytes/macrophages after intravenous infusion of biochemically inert perfluorocarbon nanoemulsions [11, 19]. When PFC-NEs were applied 1 day after MI (60-minute ischemia/reperfusion) in the rat we found—as in previous experiments in mice [11]—the fluorine label to be closely associated with the injured myocardium (Fig. 1A), mirroring the distribution of monocytes [19]. Surprisingly, however, when PFC-NEs were applied 3 days after MI, this resulted in the preferential labeling of the epicardial layer of the infarcted heart with only little ^{19}F labeling in the midmyocardium (Fig. 1B; supplemental online Movie 1). The epicardial ^{19}F MRI signal—undetectable in sham-operated control hearts—was larger than the infarcted area (Sirius red staining in Fig. 1B) and spanned from the site of coronary occlusion at the base to the apex of the heart (supplemental online Fig. 1). The biological half-life PFC-NE in plasma after intravenous injection was found to be only approximately 2 hours (supplemental online Fig. 2).

Similar experiments as with PFC-NEs were carried out with ρ-PFC-NE, which permitted us to microscopically study the cellular distribution of the label at higher local resolution. As shown in Figure 1C, the majority of the fluorescent label was found within the epicardial cell layer of the infarcted heart, which comprised the entire layer in a somewhat patchy fashion, with only minimal fluorescence in the midmyocardium (Fig. 1C). Consistent with the literature [3], the epicardial layer expanded to a thickness of more than 100 μm 7 days after MI.

In order to exclude the possibility that immune cells are preferentially labeled in the epicardial layer by the nanoemulsion, we repeated the ρ-PFC-NE experiments described above in GFP-transgenic rats [17]. In this experimental model, cardiomyocytes and all immune cells (monocytes, neutrophils, T cells, and B cells), but not epicardial cells, express GFP (Fig. 2B; supplemental online Fig. 3). As shown in Figure 2B, epicardial cells did not show a GFP signal, except for a few cells on the very outer cell layer; this is consistent with the immunofluorescent staining showing only rare, outer location of CD11b/c-positive cells in the epicardial layer (Fig. 2A). Upon injection of ρ-PFC-NE, however, the majority of the fluorescent label (red) in GFP-transgenic rats was localized in the mid- and inner-epicardium devoid of immune cells (Fig. 2C). Interestingly, we also found colocalization of both fluorescent labels in some cardiomyocytes in the subepicardial region (Fig. 2C). This suggests a progeny of PFC-NE-labeled cells for cardiomyocytic specification, but this event occurred at a rather low frequency (9–15 cells per midventricular slice in two hearts). Active cell division and formation of new cardiomyocytes is also supported by costaining of cardiomyocytes in the subepicardium with KI-67 (arrow in Fig. 2D). We found that approximately 46% of all epicardial cells were actively proliferating (KI-67 positive). The majority of KI-67 positive cells were positive for mesenchymal cells (CD90+, 43.2%), whereas a smaller fraction of cells expressed markers for cardiac stem cell (PDGFR-α, 4.2%; FLK-1, 1.6%; SCA-1, 0.8%; c-KIT, 0.6%) and endothelial cells (von Willebrand factor [vWF], 3%) (supplemental online Fig. 4). Consistent with the literature [5, 20], we also found expression of the cardiac developmental regulator WT-1 (Fig. 2E) and of PDGFR-α (Fig. 2F) amounting to 23% and 33% of all epicardial cells, respectively.

Characterization of Epicardial Cells by Electron Microscopy and Flow Cytometry

To further characterize the individual cell populations within the epicardial layer, labeled by PFC-NE, we analyzed the epicardial cells with TEM. As shown in Fig. 2G–2I, epicardial cells were of fibroblast/mesenchymal character by morphological criteria (large cell size and shape of nucleus) and contained significant quantities of liposomes, appearing as white holes, which in part were clustered into multilaminar endosomes (Fig. 2H). Epicardial cells also showed clathrin-coated pits (arrow in Fig. 2I), indicating active endocytosis. In addition, the PFC-NE-containing epicardial cells exhibited structural features of smooth muscle cells, such as elongated or corkscrew shape of the nucleus (Fig. 2J, 2K). The measured size distribution of the injected PFC-NEs (mean: 121.3 $\pm$ 32.6 nm) compared well with that of the PFC-containing liposomes derived from TEM measurements (mean: 127 $\pm$ 63.9 nm) (Fig. 2L); this value is similar to the diameter previously reported by us for the PFC-NE [19]. TEM analysis further revealed that the epicardial cell layer formed after MI was well vascularized. We counted the vessel density to be 293 $\pm$ 78 capillaries per mm^2 (n = 3 animals), which compares to approximately 3200 capillaries in the rat myocardium [21]. Remarkably, we also found that the capillary ultrastructure showed typical endocytic vesicular structures and is in part fenestrated (Fig. 3A).

For the positive identification of PFC-NE-labeled epicardial cells, we performed immune electromicroscopy using antibodies directed against WT-1 and CD11b/c. As shown in Figure 3B, WT-1 was mainly confined to the nucleus (Fig. 3B2) but weaker labeling was also present in cytoplasm (Fig. 3B1), which is consistent with the known cellular distribution of WT-1 [22]. WT-1-positive cells displayed cytoplasmic vesicles most likely containing PFC-NEs (Fig. 3B), which—as compared with conventional TEM (Fig. 2G–2I)—appear slightly different and less demarcated, because tissue

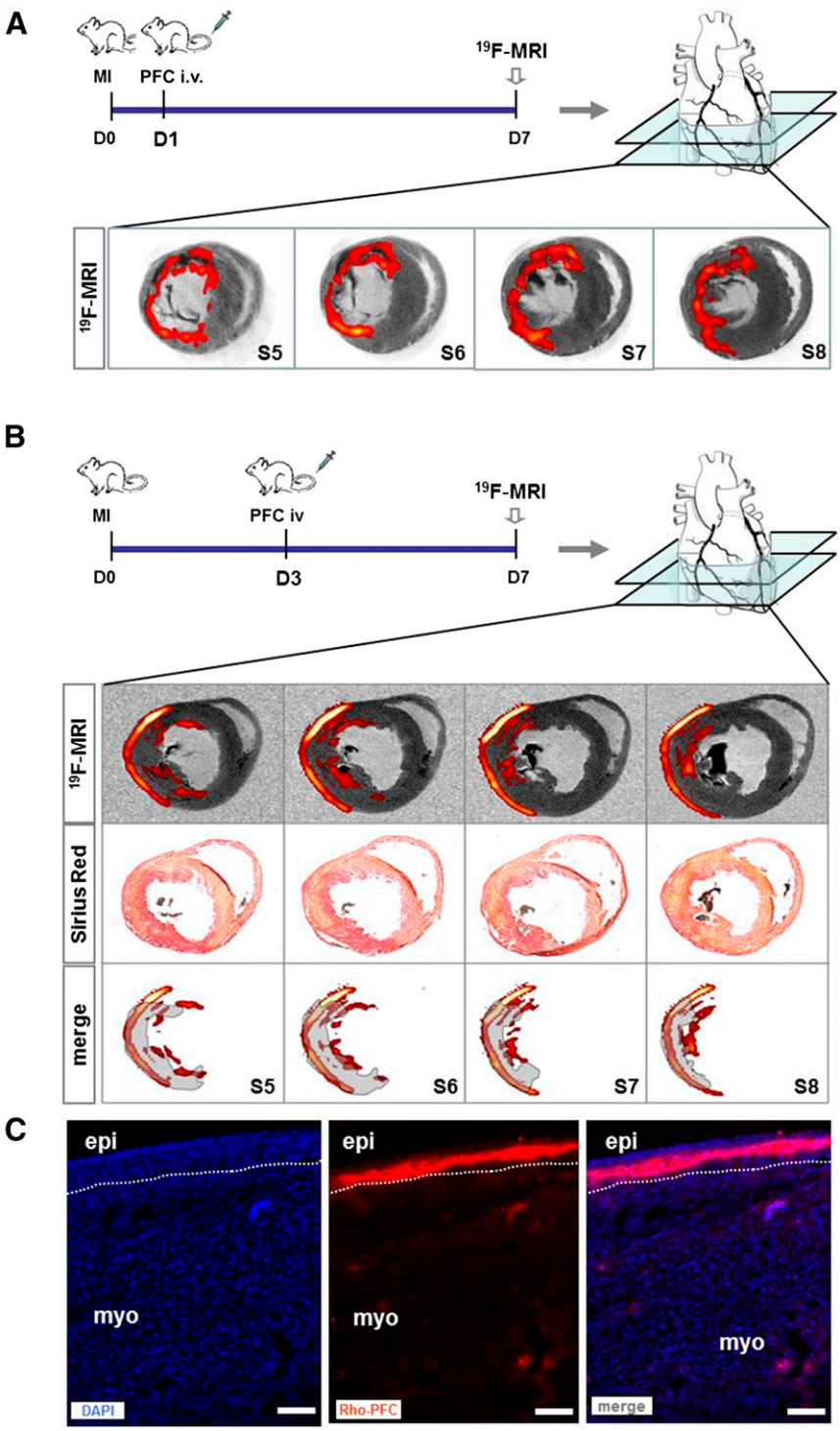

Figure 1. Labeling of the epicardium after myocardial infarction with perfluorocarbon-containing nanoemulsions (PFC-NEs). **(A):** PFC-NE (2 ml, 10% PFC) was injected into the tail vein 1 day after myocardial infarction, and ^{19}F-MRI images were taken on day 7. Fluorine label was closely located within the injured myocardium in the midventricular sections (S5–S8), mirroring the distribution of phagocytic monocytes. **(B):** When PFC-NE (2 ml, 10% PFC) was applied 3 days after MI, the fluorine signal was preferentially associated within the epicardial layer as shown for heart sections S5–S8. The ^{19}F label extended beyond the infarcted area as measured by Sirius Red staining for collagen. **(C):** Experiments identical to those shown in **(B)** were conducted with rhodamine-conjugated PFC-NE. The majority of fluorescence signal was found within the epicardial layer covering the infarcted area, whereas the midmyocardium had minor intensity. Dotted line, border between the epicardium and myocardium. Scale bars = 200 μm. Abbreviations: D0: day of myocardial infarction (60-minute ischemia/reperfusion); D1, D3, days of PFC-NE injection; D7, day of ^{19}F-MRI and fluorescence microscopy; DAPI, 4′,6-diamidino-2-phenylindole; epi, epicardium; ^{19}F-MRI, ^{19}F-magnetic resonance imaging; MI, myocardial infarction; myo, myocardium; PFC, perfluorocarbon.

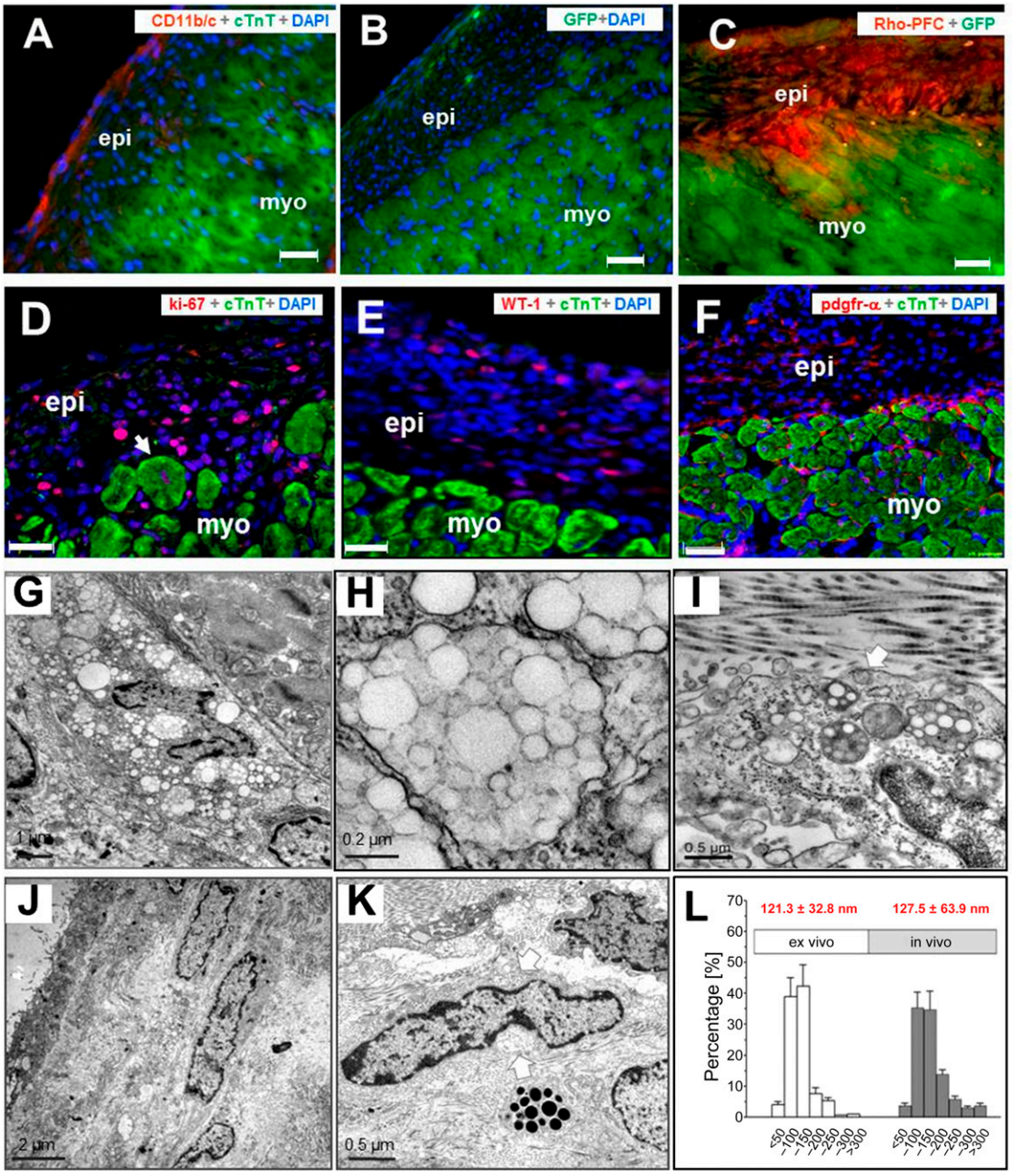

Figure 2. Analysis of the epicardium by immunohistochemistry and transmission electron microscopy (TEM). **(A):** CD11b/c-positive cells (monocytes/macrophages) represent only a small proportion of the epicardial layer and are located mostly in the very outer region of the epicardium. **(B):** Epicardial section of GFP-transgenic rat in which cardiomyocytes as well as all immune cells express GFP (supplemental online Fig. 3). Distribution of immune cells within the epicardium is similar to **(A)**. **(C):** In GFP-transgenic rats, rhodamine-coupled perfluorocarbon-containing nanoemulsion (ρ-PFC) was found mainly within the mid- and endo-epicardial layer. Some rhodamine-positive cells have migrated into the subepicardial region. **(D–F):** Epicardial cells expressed the proliferating marker KI-67 **(D)**, WT-1 **(E)**, and PDGFR-α **(F)**. **(G–I):** TEM analysis of the epicardium shows fibroblast/mesenchymal-like cells containing significant quantities of cytoplasmic liposomes (empty vesicular structures) that are partially clustered into multilaminar endosomes **(H)**. Arrow in **(I)** shows coated pits. **(J, K):** A small fraction of cells with an elongated nucleus, most likely smooth muscle cells, showed PFC-NE clusters close to the nucleus (see arrows). **(L):** Size distribution of cytoplasmic liposomes derived from TEM was similar to that of injected PFC-NE. Scale bars = 20 μm **(A–F)**. Abbreviations: cTNT, cardiac Troponin T; DAPI, 4′,6-diamidino-2-phenylindole; epi, epicardium; GFP, green fluorescent protein; myo, myocardium; pdgfr-α, platelet-derived growth factor receptor α; Rho PFC, rhodamine perfluorocarbon; WT-1, Wilms' tumor 1.

pre-embedded for immune electromicroscopy was fixed without glutaraldehyde and viewed without postembedding contrast enhancement. In general, these cells were more numerous, but heavy labeling of nuclei was often difficult to document because of the limited contrast between the specific label and the dark-gray heterochromatin. As shown in Figure 3C, the CD11b/c antibody labeled the outer membrane of cells (black grain-like precipitate) that showed no detectable PFC-NE or contained endosomes positive for CD11b/c (arrows in Fig. 3C). In addition, epicardial cells characterized by small irregular cytoplasmic

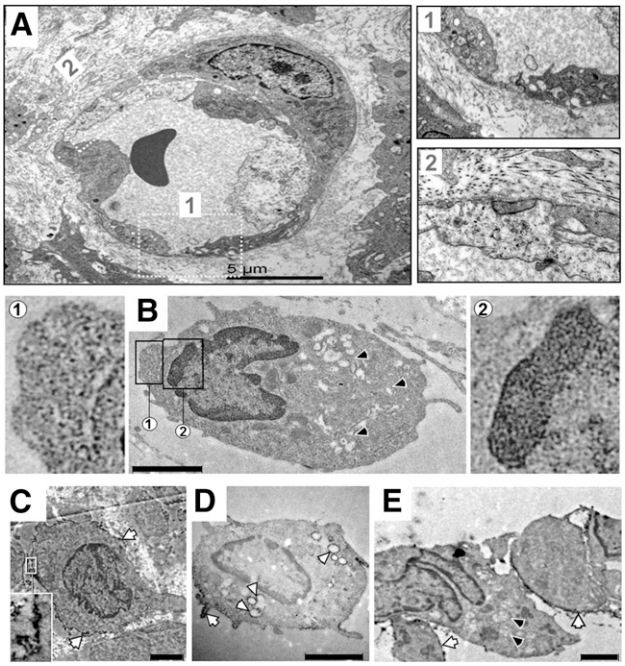

Figure 3. Vascular structure of the epicardium and immune electromicroscopy of epicardial cells. **(A):** TEM ultrastructure of a capillary within the epicardial layer shows endocytic vesicles **(A1)** and fenestration of the capillary endothelium **(A2)**. **(B):** Immune-electron microscopy of WT-1. Cells positive for WT-1 (black grain-like precipitate) stained mainly the nucleus **(B2)** and there was more dispersed labeling within the cytoplasm **(B1)**. **(C–E):** Immune-electron microscopy of CD11b/c-positive cells within the epicardium revealed cells (large central nucleus and dense cytoplasm) with typical membrane-associated activity. **(D):** Some cells showed small cytoplasmic protrusions (arrow) and endosomes encapsulated by CD11b/c-positive cell membranes (white arrows). **(E):** Intracellular liposomes were found in CD11b/c-negative cells (black arrows). Scale bars = 5 μm **(A)**; 1 μm **(B–E)**. Abbreviations: WT-1, Wilms' tumor 1.

protrusions were labeled by CD11b/c and contained endosomes surrounded by CD11b/c-positive membranes (Fig. 3D). CD11b/c-positive cells were of low frequency (4 cells of 128 counted), in line with fluorescent staining in Figure 2A. Notably, most of the PFC-NE-containing cells were found to be CD11b/c-negative (Fig. 3E).

In addition, we have characterized the cells within the epicardium labeled with PFC-NE by flow cytometry. To this end ,we have elaborated a procedure to isolate EPDCs in sufficient quantities from the heart surface using the isolated perfused heart combined with enzymatic digestion of the heart surface by collagenase (Materials and Methods). This procedure efficiently removed epicardial cells, but occasionally also reached deeper layers of the infarcted/necrotic tissue (supplemental online Fig. 5). As shown in Figure 4A, dual flow cytometry of freshly isolated epicardial cells 12 hours after ρ-PFC-NE injection revealed that the majority of the rhodamine-labeled cells were positive for mesenchymal markers such as PDGFR-α, CD73, CD105, and CD90, but negative for the myeloid marker CD45 (Fig. 4A). However, we also found CD45-positive cells (Fig. 4A), which is due to the nonuniform digestion of epicardial cells (supplemental online Fig. 5) reaching deeper layers of the infarcted heart.

Further support for the conclusion that EPDCs are preferentially labeled after intravenous ρ-PFC-NE administration comes from cytospin experiments on freshly isolated epicardial cells. As shown in Figure 4B, 4C, approximately 75% of the analyzed cells were positive for WT-1, GATA-4, KI-67, and FLK-1, whereas approximately 50% of the cells stained for PDGFR-α. Approximately 28% of the epicardial cells were positive for SM-actin. In two experiments (epicardial cells isolated 12 hours and 4 days after PFC-NE administration), approximately 90% (87% and 92%, respectively) of all cells recovered after cytospin showed positive for rhodamine fluorescence. This clearly demonstrates that the in vivo signal—either assessed by ^{19}F MRI or fluorescence—was derived from cells exhibiting characteristic features of epicardial mesenchymal cells.

Endocytic Properties of EPDC In Vitro

In the next step, we analyzed the in vitro endocytic activity of EPDCs in freshly isolated epicardial cells after coincubation with FITC-conjugated PFC-NEs. As shown in Figure 4D, epicardial cells avidly take up PFC-NEs, reaching a maximum after 50 minutes, whereas a comparable cell number of CD11b+ cells endocytosed PFC-NEs at a considerable lower rate. In order to explore whether EPDCs also take up membranes from apoptotic cells, we carried out experiments with PKH26-labeled cells derived either from rat peritoneal macrophages (PMs) or peripheral immune cells (ICs). As shown in Figure 4E, membrane fragments of PKH26-labeled apoptotic PMs and ICs were incorporated by EPDCs as shown by a clear shift of fluorescence signal at 37°C (incorporation), compared with the control at 4°C (adhesion). Mean fluorescence intensity of labeled EPDC was 2.8- and 1.8-fold above control for PM and IC, respectively.

Additional support for the endocytic activity of EPDCs comes from experiments in which we have used clodronate-containing liposomes, which are frequently used for the transient depletion of circulating monocytes [23]. In our experiments, injection of clodronate-containing liposomes (diameter, 100 nm; 25 mg/kg) on day 4 after MI not only reduced circulating monocytes (from approximately 30% to 5%, n = 3) but also significantly diminished the thickness of the epicardial layer by approximately 65% (Fig. 5D). Similarly, when isolated EPDCs were treated with clodronate-containing liposomes at a concentration of 100 μg/ml—which is similar to that reached in plasma after i.v. injection—all EPDCs underwent apoptosis.

Tracking of EPDCs In Vivo

We reasoned that studying the spatiotemporal pattern after epicardial labeling would give insights into the cell fate of in vivo-labeled EPDCs. To this end, infarcted hearts were analyzed at 4, 7, and 14 days after MI when ρ-PFC-NE was injected on day 3 (Fig. 5A). As shown in Figure 5B, the fluorescence label within the epicardial layer became gradually lost with time, whereas structures within the infarcted myocardium increased in fluorescence intensity (Fig. 5C). Interestingly, at day 7 after MI, vessel-like structures surrounding the infarcted area clearly showed rhodamine fluorescence (Fig. 5B, asterisks) comprising approximately 10% of all large vessels that stained positive for SM-actin within the infarcted area (see also Fig. 6E–6G). These experiments suggest that labeled smooth muscle cells, most likely preformed within the epicardium, trafficked to the injured myocardium and contributed to the formation of new vessels, a mechanism crucial for cardiac repair.

In an attempt to demonstrate a lineage relationship of the ρ-PFC-NE-positive cells within the epicardium and subepicardial layer, costaining with specific markers for vascular endothelial cells, smooth muscle, and cardiomyocytes was performed. For

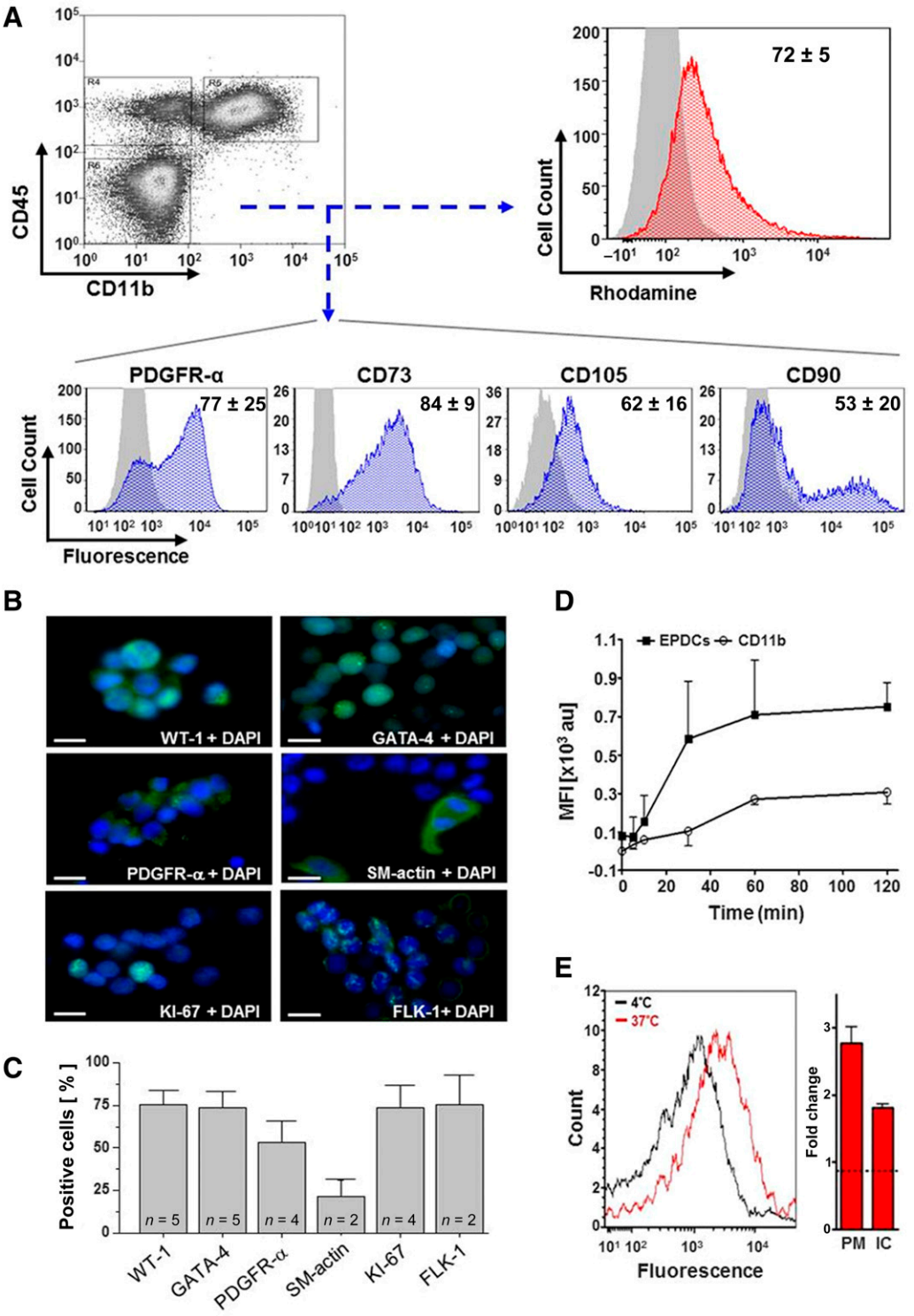

Figure 4. Cellular identities and endocytic properties of labeled EPDCs. **(A):** Fluorescence-activated cell sorting analysis epicardial cells from rhodamine-coupled perfluorocarbon-containing nanoemulsion (ρ-PFC-NE)-treated hearts that were freshly isolated by enzymatic digestion of the heart surface. Significant quantities of the epicardial cells were CD45/CD11b-negative nonimmune cells, but were labeled with ρ-PFC-NE. These cells show expression of PDGFR-α, CD73, and CD105. **(B, C):** Cytospin experiments revealed that the majority of the epicardial cells express the nuclear antigens WT-1, GATA-4, KI-67, and FLK-1. **(D):** Freshly isolated epicardial cells showed time-dependent endocytic activity when incubated with fluorescein isothiocyanate-coupled perfluorocarbon-containing nanoemulsion, which was higher than that of CD11b-positive monocytes isolated from blood. **(E):** Uptake of PKH26-labeled membrane fragments of peritoneal macrophages and peripheral immune cells by freshly isolated EPDCs. Scale bar = 10 μm **(B)**. Abbreviations: DAPI, 4′,6-diamidino-2-phenylindole; EPDCs, epicardium-derived cells; IC, peripheral immune cells; MFI, mean fluorescence intensity; PDGFR-α, platelet-derived growth factor receptor α; PM, peritoneal macrophages; WT-1, Wilms' tumor 1.

this purpose, we used an optimized tissue fixation procedure (for details, see Materials and Methods), which reduced loss of fluorescent label by the different washing steps and retained approximately 30% of the rhodamine label present in unfixed/nonpermeabilized tissue. Within the epicardial layer, we found a small fraction of rhodamine-positive cells costaining with vWF (15–30 cells per slice; Fig. 6A), but this event which was very rare in the infarcted border zone (Fig. 6C). Colocalization with SM-actin was found within the entire heart section (29–54 cells per slice in the epicardial layer, Fig. 6B; and 44–80 cells per slice in the border zone, Fig. 6D). In the necrotic area, rhodamine-positive cells were associated with large vessels (Fig. 6E) and also costained SM-actin positive arteriole- and venule-like structures (Fig. 6F, 6G). Fluorescently labeled cardiomyocytes (costaining with cTnT) could not be identified with certainty, which might be because of the partial loss of rhodamine (see above).

In a final step, we conducted similar experiments with ^{19}F-MRI to track EPDCs under in vivo conditions. Because of space restrictions within the spectrometer, we used a surface coil to follow the fate of PFC-NEs injected at day 3 after MI. Despite the limited penetration depth of the coil, the epicardial layer accumulating the ^{19}F-label could clearly be visualized in vivo (supplemental online Fig. 6, left). Furthermore, similar to the ex vivo findings, an expansion of the labeled region was observed in-vivo over time, which started from the epicardium and progressed to the inner part of the myocardium within 14 days after MI (supplemental online Fig. 6, left to right). This underlines the potential of this approach to monitor the formation of EPDCs after MI and their movement in the healing phase in a noninvasive manner.

Discussion

This study demonstrates that PFC-containing nanoemulsions administrated 3 days after myocardial infarction preferentially label EPDCs formed after myocardial infarction. This finding adds a new functionality to EPDCs formed by the heart after myocardial injury: They avidly endocytose nanoparticles with a mean size of approximately 140 nm from circulating blood, and this feature can be used for cell-tracking purposes. As to the underlying mechanism, we show that the epicardial cell layer is highly vascularized with fenestrated endothelium, which is known to permit the vascular exit of nanoparticles with an average size of 130 nm [24]. The exponential washout kinetics of injected PFC-NE thus permits pulse labeling of EPDCs formed after myocardial infarction to study their formation and fate either with fluorescently labeled or perfluorocarbon-containing nanoparticles.

Intravascular injection of fluorocarbon-containing nanoparticles was originally introduced by us to label circulating phagocytes such as CD11b$^+$ monocytes [19], and this strategy has gained widespread application for inflammation imaging [10, 19, 25]. In previous experiments, we have specified in detail the cell population in blood and tissue when the rhodamine/^{19}F-labeled nanoemulsions were applied immediately after tissue injury [11, 26]. The majority of the labeled cells in blood were CD11b$^+$ monocytes/macrophages, whereas only a marginal amount of T cells ($>$2%) were labeled [11]. In the model of lipopolysaccharide-induced lung inflammation, the most prominent ^{19}F signal again was associated with the monocyte/macrophage fraction and, to a much lesser extent, with neutrophils, whereas T and B cells were not labeled [26]. Given the well-known phagocytic activity of immune cells, it was therefore important to demonstrate that the in vivo signal observed in the present study was derived from the preferential uptake by epicardial progenitor cells with mesenchymal signature and not from resident immune cells. Several lines of evidence support this conclusion: (a) Within the epicardial cell layer, we found only rare events of CD11b$^+$ cells, and similar results were obtained in GFP-transgenic rats, in which, aside from cardiomyocytes, all immune cells were fluorescently labeled. Importantly, the majority of the epicardial cells in GFP-transgenic rats are devoid of GFP expression, and it is this cell fraction that becomes labeled by the rhodamine-conjugated nanoparticles (Fig. 2A–2C). (b) Flow cytometric analysis of freshly isolated epicardial cells, obtained after enzymatic digestion of the heart surface, showed that a significant fraction of cells that were negative either for CD45 or CD11b contained rhodamine-marked nanoparticles. These labeled cells were positive for mesenchymal markers such as PDGFR-α, CD73, CD105, and CD90 (Fig. 4A) [3]. Cytospin experiments of the freshly isolated epicardial cells revealed that approximately 75% of the cells express the nuclear transcription factor WT-1 and GATA-4, as well as KI-67 and FLK-1; approximately 60% were positive for PDGFR-α (Fig. 4B). Cells positive for WT-1 also were positive for nanoparticle uptake as shown by immune electromicroscopy (Fig. 3B).

The data of this study demonstrate that the time of infusion of the PFC-containing nanoemulsion is of crucial importance and determines which cell type within the infarcted heart is labeled: Injection immediately after myocardial infarction permits the imaging of local macrophages because circulating monocytes endocytose the NE, which thereafter migrate into the injured myocardium [11]. However, when the nanoemulsion is applied 3 days after myocardial infarction, at a point in time when monocyte infiltration into the heart is almost completed and the epicardial layer has reached its maximal thickness, it is the EPDC that preferentially takes up the nanoemulsions within the heart. This feature may permit future studies to discriminate in vivo these two cell populations within the infarcted heart by using ^{19}F-MRI.

The epicardial layer has been reported to contain a heterogeneous cell population [5]. In line with this notion, we found that a certain subpopulation within the epicardial layer formed after MI stained positive for WT-1, PDGFR-α, and KI-67 (Fig. 2D–2F). Surprisingly, according to morphological criteria, we found in TEM (Fig. 2J, 2K) and in cytospin experiments (Fig. 4B, 4C) clear evidence for the epicardial presence of preformed smooth muscle cells. These smooth muscle cells contained PFC nanoparticles as observed by TEM and by rhodamine fluorescence using immunofluorescence staining (Fig. 6B). In kinetic studies extending more than 7 days, we also were able to demonstrate that smooth muscle cells residing with the epicardial cell layer migrate over time into the underlying necrotic tissue and participate in the formation of large and small vessels forming in the infarct border zone (Fig. 5B, 5E). This finding demonstrates that EPDC-derived smooth muscle cells actively contribute to the revascularization of the infarcted heart.

By recapitulating an embryonic program, the epicardium may also signal toward heart regeneration [2]. However, the frequency of newly formed cardiomyocytes from EPDC in the adult mammalian heart is rather low. Even when stimulated with thymosin-β4, the rate of newly formed cardiomyocytes was below 1% [2]. Similarly, we found some evidence for the formation of cardiomyocytes as evidenced by KI-67-positive cardiomyocytes in the subepicardium and costaining of GFP-labeled cardiomyocytes with rhodamine. Again, the frequency of this event was rather low in the infarcted rat heart.

Perfluorocarbon-containing nanoemulsions are nontoxic and have already been used in the clinic as a blood substitute [27]. We

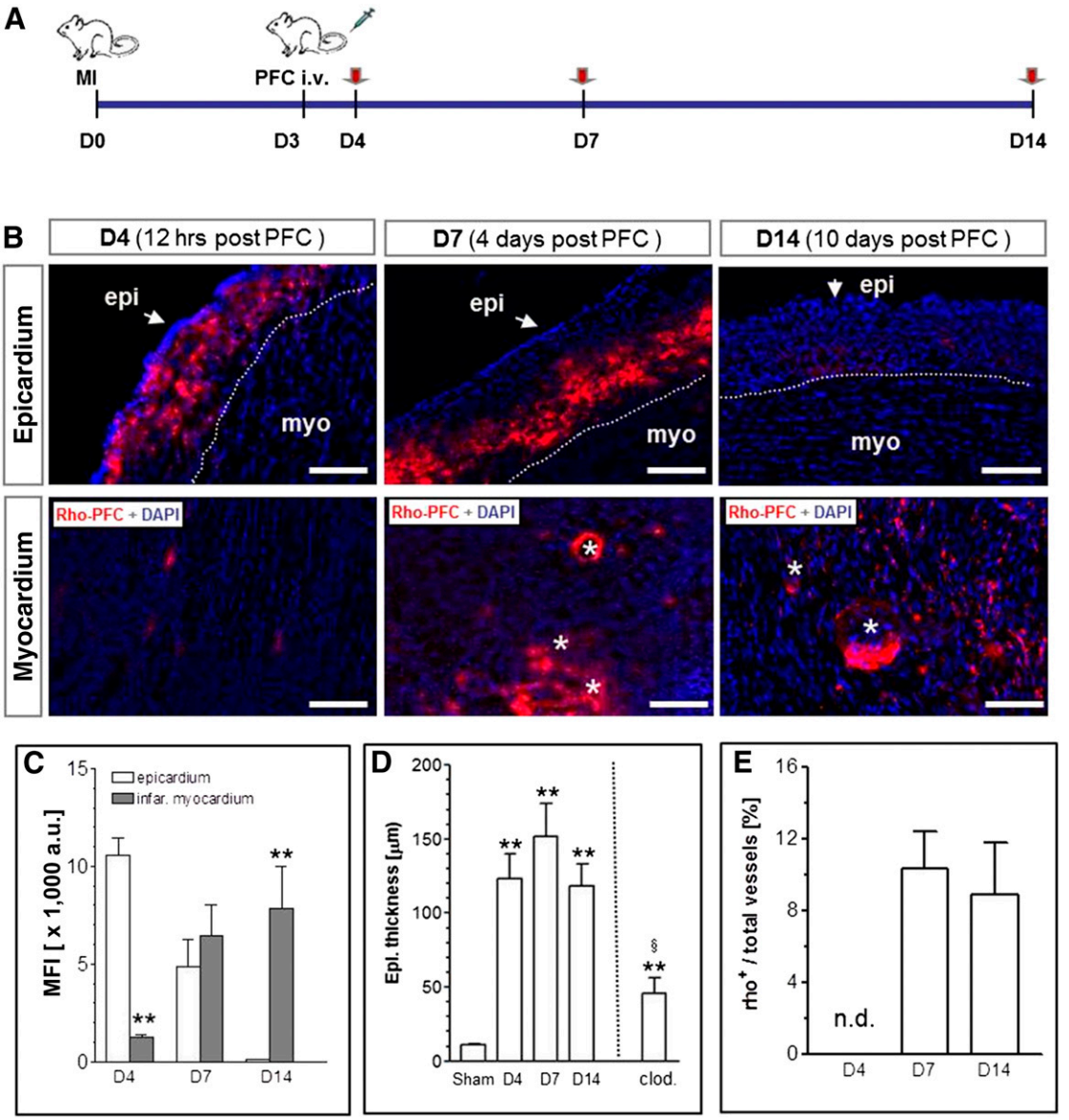

Figure 5. Functional characterization of epicardial cells. **(A):** Experimental scheme showing that rhodamine-coupled perfluorocarbon-containing nanoemulsion (ρ-PFC) were injected on day 3 after myocardial infarction (MI), and individual heart samples were analyzed (indicated by red arrows) after 12 hours (D4), 4 days (D7), and 10 days (D14), respectively. **(B):** Fluorescence microscopic analysis on D4, D7, and D14 revealed that the rhodamine label within the epicardial layer becomes gradually lost over time, whereas fluorescence intensity within the infarcted myocardium proportionally increased, suggesting migration of ρ-PFC-NE-labeled cells from their origin to the infarcted myocardium. Notably, the rhodamine signal was found inside the infarcted myocardium on D7 and D10, which showed vessel-like structures with diameter of 50–100 μm (asterisks). **(C):** Distribution of fluorescence signal between epicardium and infarcted myocardium on D4, D7, and D14. **(D):** Epicardial thickness in sham-operated animals and at D4, D7, and D14 after MI. Epicardial thickness was considerably reduced by clodronate-containing liposomes. Clodronate (25 mg/kg) was i.v.-injected on day 4 after MI, and the epicardium was analyzed on day 7. **(E):** Approximately 10% of the morphologically identified vessels within the infarct area were positive for rhodamine. Scale bars = 100 μm **(B)** top, 20 μm **(B)** bottom. ** , $p < .01$ compared with epicardium in **(C)** and to sham in **(D)**; $n = 4$. §, $p < .01$ compared with D7 without clodronate treatment in **(D)**. Abbreviations: a.u., arbitrary units; clod., clodronate; D4, analyzed after 12 hours; D7, analyzed after 4 days; D14, analyzed after 10 days; DAPI, 4′,6-diamidino-2-phenylindole; epi, epicardial layer; infar., infarcted; MFI, mean fluorescence intensity; MI, myocardial infarction; myo, myocardium; n.d., not determined; Rho PFC, rhodamine perfluorocarbon.

recently demonstrated the feasibility of monocyte imaging with ^{19}F-MRI in a pig model of MI in a clinical scanner at 3 Tesla when the nanoemulsions were applied immediately after injury [28]. As discussed above, the time of PFC application after MI is critical for the labeling and imaging of either invading monocytes/macrophages or EPDC. Thus, depending on the time of application of the PFC nanoemulsions after MI, either the extent of inflammation can be measured and/or the magnitude of the epicardial layer formed after MI can be assessed. Measurement of these two parameters may carry important information as to the healing process of the injured heart. It should be kept in mind, however, that the in vivo resolution of ^{19}F-MRI is much lower than the ex-vivo resolution of fluorescence microscopy. Furthermore, tracking lineage specification will always require specific antibodies because NMR can only locate

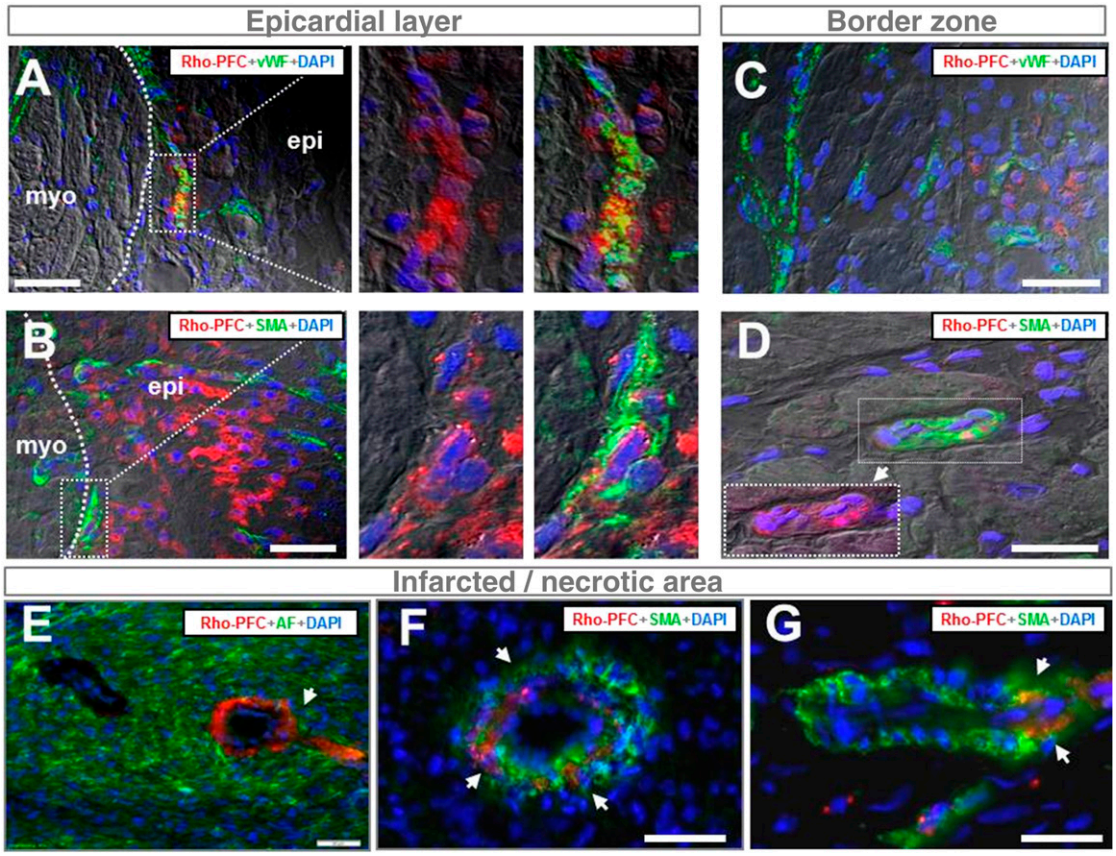

Figure 6. Lineage specification of PFC-NE-containing epicardial cells. **(A–D):** Both vWF (endothelial marker)- and SM-actin (smooth muscle cell marker)-positive rhodamine perfluorocarbon-containing nanoemulsion-containing cells (ρ-PFC) were found in the epicardium adjacent the myocardium. Although vWF-positive PFC-NE-containing cells were a rather rare event, a significant number of SMA and rhodamine PFC-NE positive cells were identified. Dotted areas in **(A)** and **(B)** are magnified to the right. **(E–G):** In the necrotic area, rhodamine-positive cells were found to form vessel-like structures **(E)**, which costained with SMA of arterioles **(F)** and venules **(G)**. Overexposure-caused autofluorescence. Scale bars = 20 μm **(A–D)**, 100 μm **(E–G)**. Abbreviations: AF, autofluorescence; DAPI, 4′,6-diamidino-2-phenylindole; epi, epicardium; myo, myocardium; Rho PFC, rhodamine perfluorocarbon; SMA, SM-actin; vWF, von Willebrand factor.

the label in vivo, but not the underlying cellular structure. However, in vivo ^{19}F-MRI can clearly identify the epicardial layer formed after myocardial infarction and follows the movement of the label over time.

Clodronate-containing liposomes have been widely used experimentally for the selective depletion of circulating monocytes [23]. In the infarcted heart, clodronate has been applied to specifically study the role of monocytes in the healing process after myocardial infarction [29, 30]. The present study demonstrates that clodronate in a setting of myocardial infarction may not be monocyte-specific as is generally assumed. Because of the endocytic nature of EPDCs, clodronate-containing liposomes readily induced apoptosis of freshly isolated EPDCs and significantly reduced the thickness of the epicardial layer after MI. Thus, because of the dual cellular specificity of clodronate-containing liposomes, interpretation of functional data obtained in the infarcted heart may be difficult.

In the present study, we have used rhodamine covalently attached to the lipid shell of PFC-containing nanoparticles to track EPDC. This permitted us to follow the distribution of the label with great sensitivity. A drawback of rhodamine, however, is that after endocytosis, the rhodamine may become metabolized and is also gradually lost during normal sample procession for immunohistology, which makes costaining experiments technically demanding. Future directions for improving EPDC tracking may include, in the case of fluorescent tracking, the covalent attachment of a fluorochrome directly to the PFC. In the case of ^{19}F-MRI, improvements in hardware/software settings are likely to increase the sensitivity in the future. An additional advantage of the fluorine nucleus certainly is that it is about as MR-sensitive as protons.

Liposomes are important nanomedical devices, and many of them are already in the clinic or in clinical trials for the local delivery of chemotherapy drugs, for example, for the treatment of solid tumors [31]. Thus, the liposomal system used in the present study can also be considered to be a delivery system for the local deposition of drug-containing nanoemulsions to EPDCs. The cellular uptake of nanoparticles by EPDCs after intravenous application is facilitated by a leaky and fenestrated endothelium within the epicardial layer; in addition the size, surface charge, and lipid composition of the nanoemulsions are critical for their final cellular uptake [19].

Conclusion

This study provides the first evidence that EPDCs formed after MI avidly endocytose nanoparticles after intravenous application and that this feature can be used for in vivo tracking of these multipotent cells. Although in the present study, liposomes were loaded with perfluorocarbons, the same system may be used in the future for the local delivery of substances that drive EPDCs into the cardiomyocytic lineage. Currently, however, little is known

about mediators, drugs, miRNA, etc. that can stimulate cardiomyogenesis in EPDCs in sufficient magnitude. Should this information become available, the liposomal drug delivery system described in this study may permit the delivery of instructive signals to EPDCs by an intravenous route.

Acknowledgments

We thank M. Nissen for technical assistance in immune electromicroscopy and Drs. S. Haberlorn and T. Schmidt for their help with some MRI scanning experiments. The study was supported by Research Council of the Heinrich-Heine-University Grant FoKo 23/2013 (to Z.D.), German Research Council Deutsche Forschungsgemeinschaft Grant SFB 1116/B01 (to J.S.), and the Cardiovascular Research Institute Düsseldorf, Medical Faculty, University of Düsseldorf, Germany.

Author Contributions

Z.D.: design, collection and/or assembly of data, data analysis and interpretation; S.T., C.Q., D.F., C.J., K.Z., H.-J.B., C.G., R.S., and U.F.: collection and/or assembly of data; J.S.: conception and design, manuscript writing, final approval of manuscript.

Disclosure of Potential Conflicts of Interest

J.S. is CEO of Crozet-Medical GmbH (Duesseldorf, Germany), has uncompensated intellectual property rights for inflammation imaging within Crozet-Medical GmbH, and has uncompensated research funding by the German Research Council (Deutsche Forschungsgemeinschaft) on purinergic signaling on T cells. The other authors indicated no potential conflicts of interest.

References

1 Gittenberger-de Groot AC, Winter EM, Bartelings MM et al. The arterial and cardiac epicardium in development, disease and repair. Differentiation 2012;84:41–53.
2 Smart N, Bollini S, Dubé KN et al. De novo cardiomyocytes from within the activated adult heart after injury. Nature 2011;474:640–644.
3 van Wijk B, Gunst QD, Moorman AFM et al. Cardiac regeneration from activated epicardium. PLoS One 2012;7:e44692.
4 van Tuyn J, Atsma DE, Winter EM et al. Epicardial cells of human adults can undergo an epithelial-to-mesenchymal transition and obtain characteristics of smooth muscle cells in vitro. Stem Cells 2007;25:271–278.
5 Bollini S, Vieira JM, Howard S et al. Reactivated adult epicardial progenitor cells are a heterogeneous population molecularly distinct from their embryonic counterparts. Stem Cells Dev 2014;23:1719–1730.
6 Zhou B, Honor LB, He H et al. Adult mouse epicardium modulates myocardial injury by secreting paracrine factors. J Clin Invest 2011;121:1894–1904.
7 Tao J, Doughman Y, Yang K et al. Epicardial HIF signaling regulates vascular precursor cell invasion into the myocardium. Dev Biol 2013;376:136–149.
8 Azene N, Fu Y, Maurer J et al. Tracking of stem cells in vivo for cardiovascular applications. J Cardiovasc Magn Reson 2014;16:7.
9 Bulte JW, Kraitchman DL. Iron oxide MR contrast agents for molecular and cellular imaging. NMR Biomed 2004;17:484–499.
10 Ahrens ET, Flores R, Xu H et al. In vivo imaging platform for tracking immunotherapeutic cells. Nat Biotechnol 2005;23:983–987.
11 Flögel U, Ding Z, Hardung H et al. In vivo monitoring of inflammation after cardiac and cerebral ischemia by fluorine magnetic resonance imaging. Circulation 2008;118:140–148.
12 Jacoby C, Borg N, Heusch P et al. Visualization of immune cell infiltration in experimental viral myocarditis by (19)F MRI in vivo. MAGMA 2014;27:101–106.
13 van Heeswijk RB, De Blois J, Kania G et al. Selective in vivo visualization of immune-cell infiltration in a mouse model of autoimmune myocarditis by fluorine-19 cardiac magnetic resonance. Circ Cardiovasc Imaging 2013;6:277–284.
14 Flögel U, Burghoff S, van Lent PL et al. Selective activation of adenosine A2A receptors on immune cells by a CD73-dependent prodrug suppresses joint inflammation in experimental rheumatoid arthritis. Sci Transl Med 2012;4:146ra108.
15 Flögel U, Su S, Kreideweiss I et al. Noninvasive detection of graft rejection by in vivo (19) F MRI in the early stage. Am J Transplant 2011;11:235–244.
16 Ye YX, Basse-Lüsebrink TC, Arias-Loza PA et al. Monitoring of monocyte recruitment in reperfused myocardial infarction with intramyocardial hemorrhage and microvascular obstruction by combined fluorine 19 and proton cardiac magnetic resonance imaging. Circulation 2013;128:1878–1888.
17 Hakamata Y, Murakami T, Kobayashi E. "Firefly rats" as an organ/cellular source for long-term in vivo bioluminescent imaging. Transplantation 2006;81:1179–1184.
18 Flögel U, Jacoby C, Gödecke A et al. In vivo 2D mapping of impaired murine cardiac energetics in NO-induced heart failure. Magn Reson Med 2007;57:50–58.
19 Temme S, Bönner F, Schrader J et al. 19F magnetic resonance imaging of endogenous macrophages in inflammation. Wiley Interdiscip Rev Nanomed Nanobiotechnol 2012;4:329–343.
20 Noseda M, Harada M, McSweeney S et al. PDGFRα demarcates the cardiogenic clonogenic Sca1+ stem/progenitor cell in adult murine myocardium. Nat Commun 2015;6:6930.
21 Vetterlein F, dal Ri H, Schmidt G. Capillary density in rat myocardium during timed plasma staining. Am J Physiol 1982;242:H133–H141.
22 Niksic M, Slight J, Sanford JR et al. The Wilms' tumour protein (WT1) shuttles between nucleus and cytoplasm and is present in functional polysomes. Hum Mol Genet 2004;13:463–471.
23 van Rooijen N, Bakker J, Sanders A. Transient suppression of macrophage functions by liposome-encapsulated drugs. Trends Biotechnol 1997;15:178–185.
24 Dejana E, Vestweber D. The role of VE-cadherin in vascular morphogenesis and permeability control. Prog Mol Biol Transl Sci 2013;116:119–144.
25 Ruiz-Villalba A, Ziogas A, Ehrbar M et al. Characterization of epicardial-derived cardiac interstitial cells: Differentiation and mobilization of heart fibroblast progenitors. PLoS One 2013;8:e53694.
26 Ebner B, Behm P, Jacoby C et al. Early assessment of pulmonary inflammation by 19F MRI in vivo. Circ Cardiovasc Imaging 2010;3:202–210.
27 Spahn DR, Waschke KF, Standl T et al. Use of perflubron emulsion to decrease allogeneic blood transfusion in high-blood-loss noncardiac surgery: Results of a European phase 3 study. Anesthesiology 2002;97:1338–1349.
28 Bönner F, Merx MW, Klingel K et al. Monocyte imaging after myocardial infarction with 19F MRI at 3 T: A pilot study in explanted porcine hearts. Eur Heart J Cardiovasc Imaging 2015;16:612–620.
29 van Amerongen MJ, Harmsen MC, van Rooijen N et al. Macrophage depletion impairs wound healing and increases left ventricular remodeling after myocardial injury in mice. Am J Pathol 2007;170:818–829.
30 Frantz S, Hofmann U, Fraccarollo D et al. Monocytes/macrophages prevent healing defects and left ventricular thrombus formation after myocardial infarction. FASEB J 2013;27:871–881.
31 Bozzuto G, Molinari A. Liposomes as nanomedical devices. Int J Nanomedicine 2015;10:975–999.

See www.StemCellsTM.com for supporting information available online.